Solitary structures associated with parallel whistler field at magnetopause

Jyoti[1], Suresh. C. Sharma[1], R.P. Sharma[2]

[1]*Department of Applied Physics, Delhi Technological University, Shahbad Daulatpur, Bawana Road, New Delhi-110042, India*

[2]*Centre for Energy Studies, Indian Institute of Technology, Delhi, Hauz Khas, New Delhi-110016, India*

Email-id: jyotirani1506@gmail.com, Suresh321sharma@gmail.com, rpsiitd@gmail.com

Abstract

In this study, we report the developed model of solitary structures associated with whistler parallel field in magnetopause. The beam-driven whistler-mode dynamical equation has been put up with the expectation that it will expand from noise level due to beam energy to large amplitude and then localize due to nonlinear effects due to ponderomotive force. Thus, whistler waves will ultimately occur in a turbulent state. The results of the numerical simulation show that the intense localized structure and power spectra are considered to be responsible for the heating and acceleration of plasma particles. The transverse scale size of the localized structure is of the order of electron inertial length.

I. Introduction

Plasma supports a various wave modes like whistler wave mode, alfven wave, magnetosonic wave, lower hybrid wave (LHW), upper hybrid wave (UHW) and ion acoustic wave. These waves play significant role in the energization and particle acceleration. Whistler waves are found to play an eminent role in the astrophysical plasmas. Whistler waves are right-handed circularly polarized wave with frequency below the electron cyclotron frequency. In the present study, we will study the observations of solitary structures associated with whistler parallel field in magnetopause. Evolution of localized structures also represents the transfer of energy from larger scale to smaller scale and the corresponding power spectrum has been calculated. The formation of the thermal tail of energetic particles is caused by energy distribution at lower scales. Basic formulation of theoretical model mentioned in Sec. II in which model equations are solved numerically. The numerical simulation is discussed in Sec. III. In Sec. IV, Results and conclusion are presented.

II. Theoretical Model

A) Whistler wave

The dynamical equation for whistler wave (2D plane), which is propagating in the x-z plane with wave vector $\vec{k} = k_x\hat{x} + k_z\hat{z}$, in a magnetized plasma with an ambient magnetic field along

the z-axis is derived by two fluid models, equation of motion and wave equation, which is given by

$$\frac{-\partial^2 E_z}{\partial t^2}-\lambda_e^4\frac{\partial^6 E_z}{\partial x^4\partial t^2}-\lambda_e^4\frac{\partial^6 E_z}{\partial z^4\partial t^2}-2\lambda_e^4\frac{\partial^6 E_z}{\partial x^2\partial z^2\partial t^2}+2\lambda_e^2\frac{\partial^4 E_z}{\partial x^2\partial t^2}+2\lambda_e^2\frac{\partial^4 E_z}{\partial z^2\partial t^2}+\lambda_e^4\omega_{ce}^2\left(\frac{\partial^4 E_z}{\partial z^2\partial x^2}+\frac{\partial^4 E_z}{\partial z^4}\right)=0. \quad (1)$$

Now, assuming envelope solution for eq. (1) $\tilde{E}_z = E_z(x,z,t)e^{i(k_{0x}\hat{x}+k_{0z}\hat{z}-\omega_0 t)}$, we obtained:-

$$\begin{aligned}&2i\omega_0(1+\lambda_e^4k_{0x}^4+\lambda_e^4k_{0z}^4+2\lambda_e^2k_{0x}^2+2\lambda_e^2k_{0z}^2)\frac{\partial E_z}{\partial t}+(-4\omega_0^2\lambda_e^4k_{0x}^2)\frac{\partial^2 E_z}{\partial x^2}+(4\lambda_i^2v_A^2k_{0z}^2-4\omega_0^2\lambda_e^4k_{0z}^2)\frac{\partial^2 E_z}{\partial z^2}+\\&2i(-2\omega_0^2k_{0x}^3\lambda_e^4+2\omega_0^2k_{0x}k_{0z}^2\lambda_e^4+2\omega_0^2\lambda_e^2k_{0x}+k_{0x}k_{0z}^2\lambda_i^2v_A^2)\frac{\partial E_z}{\partial x}+\\&2i(-2\omega_0^2k_{0z}^3\lambda_e^4+2\omega_0^2k_{0z}k_{0x}^2\lambda_e^4+2\omega_0^2\lambda_e^2k_{0z}+k_{0z}k_{0x}^2\lambda_i^2v_A^2+2k_{0z}^3\lambda_i^2v_A^2)\frac{\partial E_z}{\partial z}+\\&(4\lambda_i^2v_A^2k_{0x}k_{0z}-8\omega_0^2k_{0z}k_{0x}\lambda_e^4)\frac{\partial^2 E_z}{\partial x\partial z}+\\&(9\lambda_i^2v_A^2k^2k_{0z}^2)\frac{\delta n}{n_0}E_z=0.\end{aligned} \quad (2)$$

where k_{0x}, k_{0z} are whistler wave vector components related to the background magnetic field are given below. $k_0^2=k_{0x}^2+k_{0z}^2$ and λ_e, λ_i are the skin depth of electrons and ions. And, $v_A\left(=\frac{B_0^2}{4\pi n_0 m_i}\right)$ is the speed of the Alfven waves.

B) Ion Acoustic wave

Consider a low-frequency ion-acoustic wave travelling along the z-axis parallel to the background magnetic field $\vec{B}_0$ i.e., $\vec{B}_0=B_0\hat{z}$, $\vec{k}=k_z\hat{z}$. Using the equations of motion for electrons and ions, as well as the continuity equation, the dynamical equation for IAW was obtained. $$\left(\frac{\partial^2 n}{\partial t^2}-c_s^2\frac{\partial^2}{\partial z^2}\right)\left(\frac{n}{n_0}\right)=-\frac{\partial}{\partial z}\left[\frac{F_{ez}+F_{iz}}{m_i}\right] \quad (3)$$

where $c_s\left(=\frac{k_B(T_e+T_i)}{m_i}\right)^{1/2}$ is the speed of IAW, k_B is the Boltzmann constant. T_e, T_i are the temperature of electron and ion, respectively. F_{ez} (F_{iz}) is the component of ponderomotive force in *z*-direction produced by whistler wave. Now, the Ponderomotive force of the whistler wave is defined as, $\vec{F}_j=-m_j(\vec{v}_j*.\vec{\nabla})\vec{v}_j+\frac{q_j}{c}(\vec{v}_j*\times B_w).$ Here $'j'$ denote the charged species i.e., electron and ion. Thus m_j, v_j and q_j are the mass, velocity, and charge of the electron and ion, respectively. *c* is the speed of light and B_w is the magnetic field due to the whistler wave. Obtaining the ponderomotive force components owing to whistler wave and then put their values in Eq. (3). We get

$$\left(\frac{\partial^2}{\partial t^2}-c_s^2\frac{\partial^2}{\partial z^2}\right)\left(\frac{n}{n_0}\right)=\begin{pmatrix}-\dfrac{e^2(\alpha_1^2+2\alpha_1\omega_{ce}^2+\omega_0^2\omega_{ce}^2)}{m_e m_i(\omega_0^2-\omega_{ce}^2)\alpha_1^2}\dfrac{\partial^2}{\partial z^2}|E_z|^2\\ +\dfrac{e^2}{m_e m_i\omega_0^2}\dfrac{\partial^2}{\partial z^2}|E_z|^2+\dfrac{3e^2\omega_{ci}^2}{m_e m_i\omega_0^2}\dfrac{\partial^2}{\partial z^2}|E_z|^2\end{pmatrix}. \quad (4)$$

Equations (2) and (4) are normalized by using these parameters:

$$t_n=1/\omega_0. \qquad n(x,z)=|E_z(x,z)|^2. \qquad x_n=\frac{2i(-2\omega_0^2k_{0x}^3\lambda_e^4+2\omega_0^2k_{0x}k_{0z}^2\lambda_e^4+2\omega_0^2\lambda_e^2k_{0x}+k_{0x}k_{0z}^2\lambda_i^2v_A^2)}{2\omega_0(1+\lambda_e^4k_{0x}^4+\lambda_e^4k_{0z}^4+2\lambda_e^2k_{0x}^2+2\lambda_e^2k_{0z}^2)}.$$

$$z_n=\frac{2i(-2\omega_0^2k_{0x}^3\lambda_e^4+2\omega_0^2k_{0x}k_{0z}^2\lambda_e^4+2\omega_0^2\lambda_e^2k_{0x}+k_{0x}k_{0z}^2\lambda_i^2v_A^2+2k_{0z}^3\lambda_i^2v_A^2)}{2\omega_0(1+\lambda_e^4k_{0x}^4+\lambda_e^4k_{0z}^4+2\lambda_e^2k_{0x}^2+2\lambda_e^2k_{0z}^2)}.$$

$$E_n=\left[\frac{c_s^2m_em_i(\omega_0^2-\omega_{ce}^2)\alpha_1^2t_n^2\omega_0^2}{n_0e^2\left\{(\alpha_1^2+2\alpha_1\omega_{ce}^2+\omega_0^2\omega_{ce}^2)+(1+3\omega_{ci}^2)(\omega_0^2-\omega_{ce}^2)\alpha_1^2\right\}z_n^2}\right]^{\frac{1}{2}}$$

After normalization, the equation in normalized dimensionless form is given as

$$i\frac{\partial E_z'}{\partial t'}+c_1\frac{\partial^2E_z'}{\partial x'^2}+c_2\frac{\partial^2E_z'}{\partial z'^2}+i\frac{\partial E_z'}{\partial x'}+i\frac{\partial E_z'}{\partial z'}+c_3\frac{\partial^2E_z'}{\partial x'\partial z'}+c_4|E_z|^2E_z'+2i\gamma'E_z'=0. \quad (5)$$

where Eq. (5) represents the normalized dynamical equation for the whistler wave which leads the turbulence. Here $\gamma'\left(\gamma'=\frac{\gamma}{\omega_0}\right)$ is the normalized growth rate, which is introduced to describe the beam instability driving the beam-driven whistler wave. The growth rate of the beam-driven whistler i.e., $\gamma'>0$ is incorporated phenomenologically and its value consistent with the observations reported by Zhao et al. will be used in simulations here. Where,

$$c_1=\frac{-4\omega_0^2\lambda_e^4k_{0x}^2}{2\omega_0(1+\lambda_e^4k_{0x}^4+\lambda_e^4k_{0z}^4+2\lambda_e^2k_{0x}^2+2\lambda_e^2k_{0z}^2)x_n^2}. \qquad c_2=\frac{(4\lambda_i^2v_A^2k_{0z}^2-4\omega_0^2\lambda_e^4k_{0z}^2)}{2\omega_0(1+\lambda_e^4k_{0x}^4+\lambda_e^4k_{0z}^4+2\lambda_e^2k_{0x}^2+2\lambda_e^2k_{0z}^2)z_n^2}.$$

$$c_3=\frac{(4\lambda_i^2v_A^2k_{0x}k_{0z}-8\omega^2k_{0z}k_{0z}\lambda_e^4)}{2\omega_0(1+\lambda_e^4k_{0x}^4+\lambda_e^4k_{0z}^4+2\lambda_e^2k_{0x}^2+2\lambda_e^2k_{0z}^2)z_nx_n}. \qquad c_4=\frac{9\lambda_i^2v_A^2k^2k_{0z}^2}{2\omega_0(1+\lambda_e^4k_{0x}^4+\lambda_e^4k_{0z}^4+2\lambda_e^2k_{0x}^2+2\lambda_e^2k_{0z}^2)}.$$

III. Numerical Simulation

Numerical simulation for the Eq. (5) is carried out by using a 2D pseudospectral method in a periodic box having domain $(10\pi\times10\pi)$ and $(256)^2$ grid points. The imposed initial condition for numerical simulation is given by- $E_z(x,z)=a_0(1+\beta\cos(\alpha_x x))(1+\beta\cos(\alpha_z z))$. (6)

Here, $a_0=0.5$ is the initial amplitude of the pump whistler wave and $\beta=0.1$ is the magnitude of the perturbed electric field. The perturbation in wave-number α_x=0.2, α_z=0.2. To begin,

the algorithm's accuracy was tested by translating the model equation into the nonlinear Schrödinger equation (NLS) and the plasmon number's consistency i.e., $N = \sum_k |E_k|^2$. This is conserved with an accuracy of the sixth decimal place. The parameters used for this numerical simulation in the magnetopause are, $B_0 = 45\text{nT}$, $n_0 = 21\text{cm}^{-3}$, $T_e = 4.2\times10^5\text{K}$, $\omega_{ce} = 7.9\times10^3\,\text{rad sec}^{-1}$ $\omega_0 = 0.2\omega_{ce}$, $\lambda_e = 1.16\times10^5\,\text{cm}$, $k\lambda_e = 0.5$, $k_{0x} = 2.98\times10^{-6}\,\text{cm}^{-1}$, $k_{0z} = 1.72\times10^{-6}\,\text{cm}^{-1}$, $x_n = 0.9\lambda_e$, $z_n = 1.32\lambda_e$, $t_n = \omega_0^{-1}$. From these parameters, we obtain $c_1 = -0.2681$, $c_2 = 1.0080$, $c_3 = 2.4398$.

IV. Results and conclusion

We report the solitary structures by developing theoretical model that indicates the presence of turbulence formed due to nonlinear interaction of high-frequency whistler wave and low-frequency IAW. Due to large amplitude whistler waves, ponderomotive force components emerge, which are included into IAW's nonlinear dynamics. The results of the numerical simulation of Eq. (5) applicable to magnetopause region are presented here. Fig. 1 depicts the evolution of coherent structures with time. We also presented the results of power spectra in Fig. 2, We just give the scaling of reference lines by red and green colour for inertial range and dissipation range respectively, and actual power spectra is given by solid curve line.

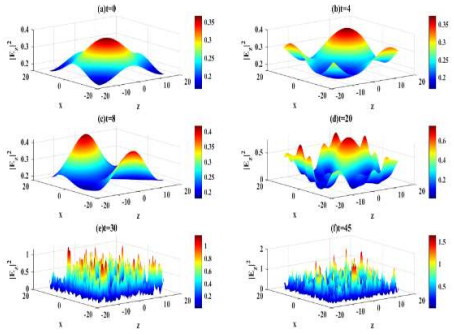

Figure.1
The normalized field evolution of whistler wave

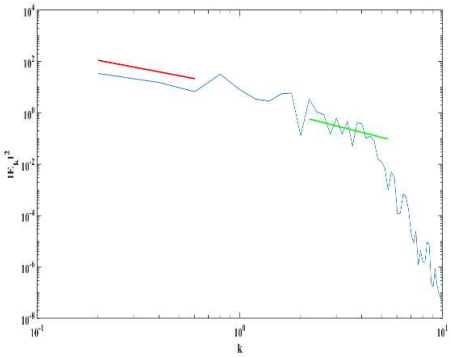

Figure.2
Power spectra of whistler wave at t=52

Acknowledgement

The authors are thankful to the UGC for providing financial assistance under SRF fellowship.

References

[1]Zhao et al. (2021), Observations of the beam-driven whistler-mode waves in the magnetic reconnection region at the dayside magnetopause Journal of Geophysical Research: Space Physics, **126,** https://doi.org/10.1029/2020JA028525.